Motion Control of a Soft-Actuated Modular Manipulator

Erik H. Skorina, Weijia Tao, Fuchen Chen, Ming Luo, and Cagdas D. Onal

***Abstract*— Soft pneumatic actuators can allow robotic manipulators to interact safely in complex environments in close proximity to humans, but work still needs to be done controlling them more effectively. We explore this area by introducing a 2-degree of freedom (DoF) universal joint module actuated by three reverse Pneumatic Artificial Muscles (rPAMs) and an associated geometric Jacobian-enhanced iterative sliding mode controller. After demonstrating the effectiveness of this controller, we combine two of these modules to form a 4-DoF soft actuated manipulator. To control this modular manipulation system, we propose two controllers: a direct inverse kinematic (IK) controller and an end-effector geometric Jacobian controller. Though both controllers were validated to function effectively, the Jacobian controller was more precise (especially under payload) while the IK controller was more accurate.**

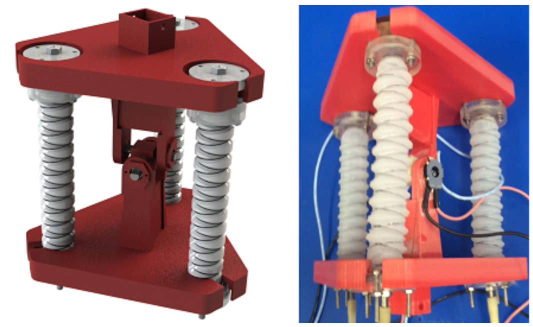

Fig. 1. A CAD model (left) and a physical prototype (right) of the 2-DoF universal joint module operated by 3 rPAM soft actuators in antagonism.

I. Introduction

Recent robotics research has seen the emergence of soft robotic arms [1]–[10]. Compared with the rigid manipulators, these soft arms are low-cost and more appropriate for human-robot interaction. Soft robotic systems commonly utilize pneumatic actuators [5]–[9]. However, motion control of pneumatic soft actuators is challenging and remains an open topic of research. First, theoretical modeling of a soft-actuated robot is not trivial, because the continuous shape of the soft actuator influenced by gravity is difficult to predict. Second, the dynamic behavior of these actuators includes a nonlinear time delay as pressurized air is introduced and released through valve commands. The control schemes of [5], [8], [9] are used on two degree freedom soft manipulators. In general, these papers directly control the input flow rates or air pressures, the infrastructure for which is often both bulky and expensive.

In our previous work [11], [12], we introduced the motion control of a 1-Degree of Freedom (DoF) joint driven by our soft pneumatic actuators, *reverse Pneumatic Artificial Muscles (rPAMs)*, which combine the properties of the McKibben Actuator and the Fluidic Elastomeric Actuator [13]–[15]. In addition, we performed precise motion control using an iterative sliding mode feedback controller augmented by a feedforward term. These controllers modulated the state of miniature solenoid binary valves connected to a constant pressure source to drive each actuator, reducing the system cost and complexity.

The study detailed in this paper provides a realistic application of soft actuators driving a modular kinematic chain in an antagonistic arrangement (as seen in Figure 1). Our approach is to operate a 2-DoF universal joint, as a representative system, controlled precisely using three rPAMs. This represents a module, which can be combined to form more complex chains. To demonstrate this, we expand the system by cascading a pair of the soft-actuated universal joints, resulting in a 4-DoF soft-actuated manipulator.

Motion control of the recently developed soft pneumatic actuators has little precedence in the literature. Due to valving hardware limitations to control multiple degrees of freedom in a compact space, our strategy is to treat the duty cycle of a pulse width modulation (PWM) signal of solenoid valves as control input to regulate a position error vector [11], inspired by methods to control rigid pneumatic piston actuators. Based on our prior work in this area, we combine an iterative sliding mode controller with a geometric Jacobian. This approach can be used for each module in the manipulation system separately, as they operate independently of each other. In addition, we present a simple direct inverse kinematic model to calculate the joint angles required to hold the upper joint horizontal at any reachable point.

The contributions of this work include:

- The improvement of our rPAM actuators to increase their reliability;
- Development of a soft-actuated 2-DoF universal joint module and associated controller to increase control pneumatic efficiency; and
- The cascading of these modules to create a 4-DoF soft actuated manipulator with associated motion controllers.

This paper starts with a description of the fabrication of the new actuator and joint. It then describes the work with the single 2-DoF joint, including kinematic modeling, updated iterative sliding mode control, and experimental results. Next, it describes work with the 4-DoF manipulator,

The authors are with the Mechanical Engineering Department and Robotics Engineering Program, Worcester Polytechnic Institute, MA 01609, USA. All correspondence should be addressed to Cagdas D. Onal `cdonal@wpi.edu`

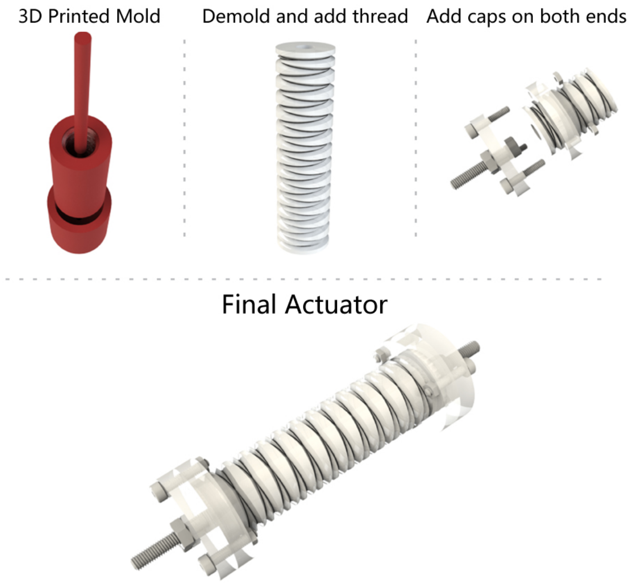

Fig. 2. The fabrication process of the soft linear actuator.

including design, modeling, inverse kinematic control, and experimental results. Finally, it ends with a discussion and future directions of research.

II. Design and Fabrication

A. Fabrication of the Soft Actuator

Our reverse pneumatic artificial muscles (rPAMs) are fabricated by molding silicone rubber (Smooth-on Dragonskin 10) in a 3-D printed mold. The step-by-step fabrication process (shown in Fig. 2) is described below:

Step 1: Insert a carbon fiber or metallic rod of appropriate diameter into the center of the body mold to create the hollow cylindrical core inside the actuator. Introduce silicone rubber into the body mold.

Step 2: After silicone rubber has cured, remove the rod inside the body mold, then remove the silicone from the body mold. Tie two symmetrical helices of thread around the cylindrical silicone rubber body guided by the grooves. Apply an outer layer of uncured silicone rubber around the threads to permanently bond the thread to the actuator.

Step 3: Sandwich each of the ends of the actuator between two layers of acrylic with an integrated vent screw to serve as pneumatic fitting and tighten to form the end caps.

This fabrication process is a simplification of our previous approach, requiring fewer fabrication steps and less molding. In addition, the acrylic and vent screw provide a more secure and repeatable interface for the input air line, which was previously the most common point of failure. These actuators can reliably withstand actuation pressures of 30 psi. In addition, the screws on either end of the actuator allow it to be easily mounted to external rigid structures.

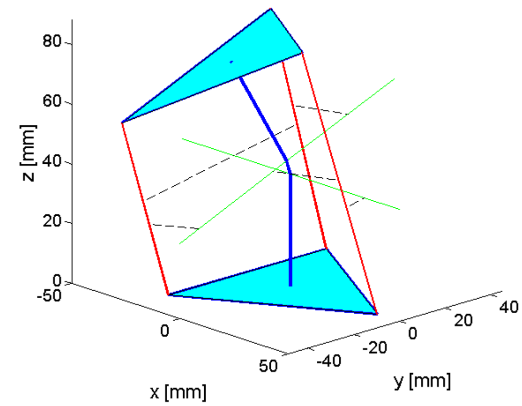

Fig. 3. Kinematic model of the 2-DoF module. Blue lines represent the links, red lines represent the actuators, green lines represent the axes of rotation, and the dashed black lines represent the moment arms for the torque generated by each actuator.

TABLE I

Kinematic parameters of the 2-DoF module model.

Change	Quantity
Z-Translation	37.5 mm
X-Rotation	θ_1
Z-Translation	5 mm
Y-Rotation	θ_2
Z-Translation	37.5 mm

B. Module Design

To demonstrate the usability of this type of actuation, we designed a universal joint to be driven by 3 rPAMs. This design methodology is scalable, to be used for controlling robotic limbs in 3-dimensional space. In addition, the coupled use of three actuators for 2-degrees of freedom (compared to two antagonistic actuators for each DoF) reduces the electronic and pneumatic infrastructure. The final prototype can be seen in Figure 1. The joint was 3-D printed out of PLA with steel axles. The two axles of the universal joint are offset slightly, and mounted with bearings to reduce friction. In addition, we used miniature potentiometers on each of the axles to provide reliable feedback for closed-loop control.

The module is designed to be longer than the nominal length of the actuators, forcing them to be pre-strained during assembly. This prevents the actuators from getting in the way of joint movement when pressure is released. Without a pre-strain that keeps the soft actuators under tension, the joint will collide with an actuator during operation, forcing it to compress and buckle outwards, thus reducing the mobility of the joint. The amount of pre-strain is not trivial to determine a priori. A trade-off seems to exist between the motion range and reliability of the modules, as a function of pre-strain. A large pre-strain value causes the joint to be unstable under increasing equal pressure inputs. Instead of staying perfectly vertical, the module would toggle between extreme angles. A moderate pre-strain eliminates this problem.

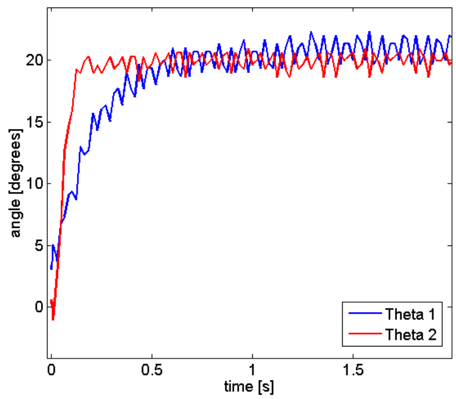

Fig. 4. The step response behavior of the controller with the 2-DoF joint. The desired angles are 20°.

III. Soft-Actuated 2-DoF Module

A. Kinematic Model and Control

For any robotic manipulator, it is useful to have a kinematic model. In the proposed module, rPAMs are mounted at radially symmetric increments of 120 degrees from each end, starting at $\begin{bmatrix} 40 \text{ mm} & 0 & 0 \end{bmatrix}$. A graphical representation of the module kinematics is shown in Fig. 3. The general parameters we used can be seen in Table I. This model was used to develop the joint control algorithm described in detail below.

Our previous work [11] resulted in an iterative sliding mode control law shown in Equation 1, which we used to control a 1-DoF joint.

$$u(t) = u(t - \Delta t) + K(\dot{e_x} + De_x), \tag{1}$$

where u is the control input, e_x and $\dot{e_x}$ are the error and its time derivative, respectively, and K and D are control coefficients. Expanding this control law to a 2-DoF system is not straightforward, as multiple actuators must interact to move the joint to a desired state. To address this, we used the assumption that changing the control input to a given actuator (representing the PWM valve duty cycle) will cause that actuator to extend or contract accordingly.

Using the kinematic model, we can determine the level of extension or contraction required from each actuator in order to move the module towards the desired angle combination. Using the forward kinematics of the 2-DoF module, the following equation can be written for the length of a given rPAM:

$$L_i = f_i(\theta_1, \theta_2), \tag{2}$$

where L_i is the length of actuator i. From here, we can calculate a Jacobian, taking partial derivatives with respect to each joint angle.

$$\begin{bmatrix} dL_a \\ dL_b \\ dL_c \end{bmatrix} = \begin{bmatrix} \frac{dL_a}{d\theta_1} & \frac{dL_a}{d\theta_2} \\ \frac{dL_b}{d\theta_1} & \frac{dL_b}{d\theta_2} \\ \frac{dL_c}{d\theta_1} & \frac{dL_c}{d\theta_2} \end{bmatrix} \begin{bmatrix} d\theta_1 \\ d\theta_2 \end{bmatrix}. \tag{3}$$

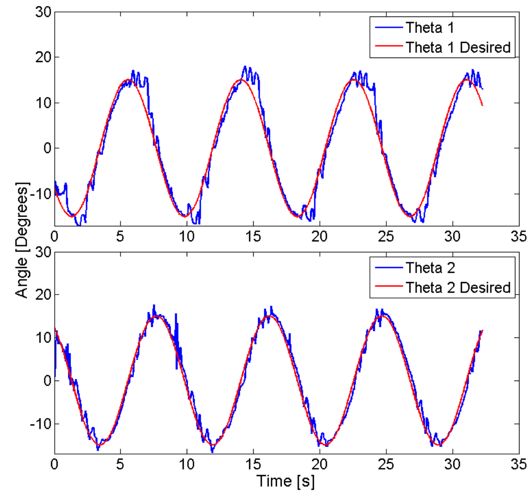

Fig. 5. The trajectory following results for the 2-DoF joint following a circular path. The period is 8.5 seconds and the amplitude is 15 degrees.

These equations are long and complicated, and thus it is computationally expensive to calculate them at every iteration of the control loop. Linearizing (3) at $\theta_1 = 0$ and $\theta_2 = 0$ (straight configuration) results in the following:

$$\begin{bmatrix} dL_a \\ dL_b \\ dL_c \end{bmatrix} = \begin{bmatrix} -0.43301 & 0.25 \\ 0.43301 & 0.25 \\ 0 & -0.5 \end{bmatrix} \begin{bmatrix} d\theta_1 \\ d\theta_2 \end{bmatrix}. \tag{4}$$

As the system has no singularities, this linearization would work for the entire workspace. Equation 4 allows us to calculate the change in actuator lengths required to match a desired change in the angles. Assuming that an increase in control input to an actuator will result in that actuator increasing in length (or at least exerting force along its axis), we can combine (4) and (1), yielding the control law:

$$\begin{aligned} \begin{bmatrix} u_a(t) \\ u_b(t) \\ u_c(t) \end{bmatrix} &= \begin{bmatrix} u_a(t-\Delta t) \\ u_b(t-\Delta t) \\ u_c(t-\Delta t) \end{bmatrix} + \\ &+ \begin{bmatrix} -0.43301 & 0.25 \\ 0.43301 & 0.25 \\ 0 & -0.5 \end{bmatrix} \begin{bmatrix} K(\dot{e}_{\theta 1} + De_{\theta 1}) \\ K(\dot{e}_{\theta 2} + De_{\theta 2}) \end{bmatrix}. \end{aligned} \tag{5}$$

B. Experimental Results

To demonstrate the effectiveness of this controller, we applied it to various trajectories. Figure 4 is a representative example of the controller trying to reach an angle combination. In this trial, θ_2 reached the desired angle of 20 degrees after less than 0.25 s while θ_1 reached the same target after 0.5 seconds. Not only was the target reached in less than a second, but the controller was capable of holding that position within ± 1 degree.

In addition, we have the controller follow a series of circular paths. These paths were generated by giving offset sinusoidal waves to each angle. An example of the controller following such a trajectory with period 8.5 s (0.1176 Hz) and

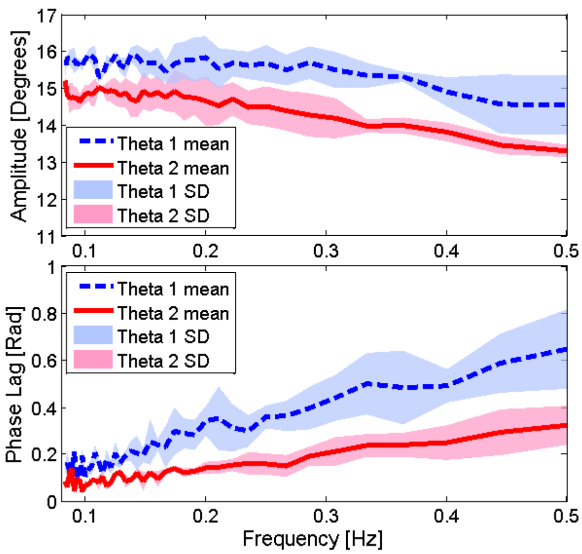

Fig. 6. A graph of the mean and standard deviation of the amplitude and phase delay of the 2-DoF joint trajectory with respect to the reference trajectory over changing frequencies. Data from three trials was used for this plot. The desired amplitude was 15 degrees.

15-degree amplitude can be seen in Figure 5. The controller follows the given trajectories with relative accuracy, while occasional oscillations are observed. This is likely a result of latent dynamic effects from the PWM-operated valves. In addition, θ_1 overshoots on both sides just after the wave switches direction.

We performed this test over a range of reference periods to determine the amplitude and phase lag of the closed loop system. We performed this experiment three times and calculated the mean and standard deviation. A plot of these results can be seen in Figure 6. The phase lag for θ_2 was consistently lower, though both increased linearly with respect to frequency. θ_1 had a slightly larger amplitude than the desired 15 degrees at lower frequencies, while θ_2 had the desired amplitude. Both amplitudes slightly decreased as the frequency increased, as expected, but remained close to the desired value for the tested frequency range.

IV. 4-DoF Modular Manipulator

In order to expand our 2-DoF module into a 4-DoF manipulator, we mounted two universal joint modules in series, as seen in Figure 7. The kinematics of the 4-DoF system utilizes the model from Table I twice, with a 30 mm vertical offset and a 60-degree rotation at the interface between the modules resulting in the model that can be seen in Figure 8.

To show the workspace of this soft-actuated manipulator, we used the kinematic model and plotted the tip location (centroid of the top plate) for combinations of joint angles between $[-\pi/6\ ,\ \pi/6]$. The resulting graph can be seen in Figure 9.

A. Control

To enact meaningful control with the manipulator, we developed two separate motion controllers. The first con-

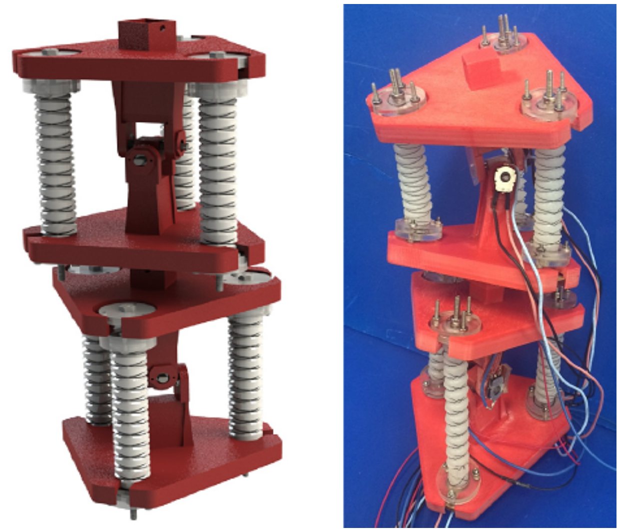

Fig. 7. A CAD model (left) and a physical prototype (right) of the 4-DoF soft actuated modular manipulator.

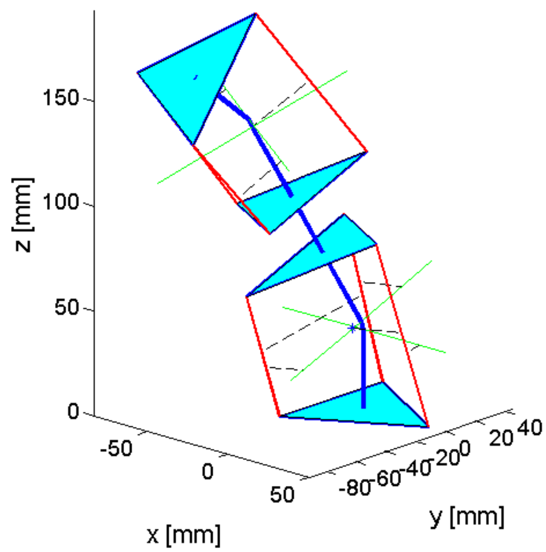

Fig. 8. Kinematics of the 4-DoF manipulator. Blue lines represent the joint, itself. Red lines represent the actuators, green lines represent the axes of rotation, and the dashed black lines represent the moment arms for the torque of each actuator around each axis.

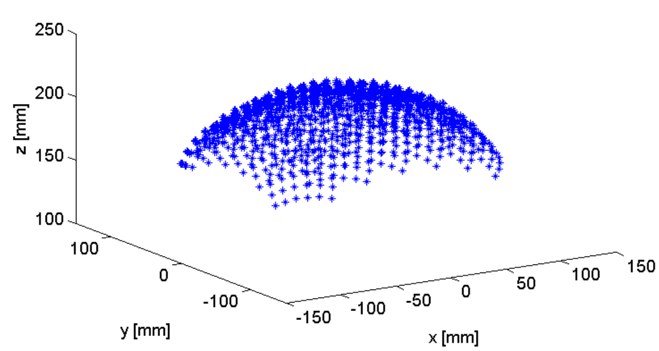

Fig. 9. A graph of the workspace of the 4-DoF manipulator when the joints can travel $\pi/6$ radians in each direction.

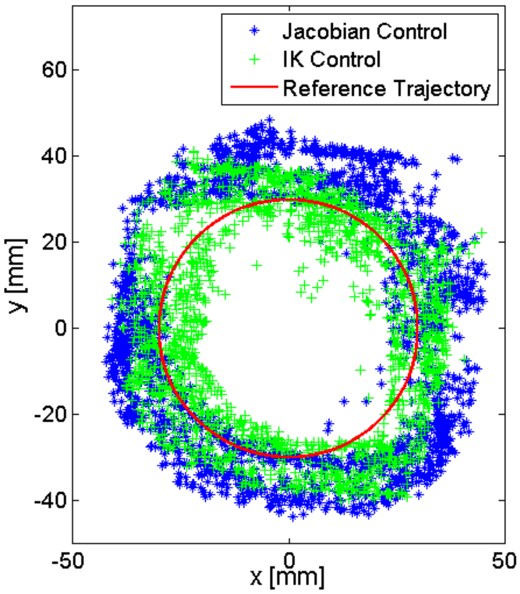

Fig. 10. The actual and reference joint trajectories of the 4-DoF manipulator end effector when using the IK versus Jacobian control.

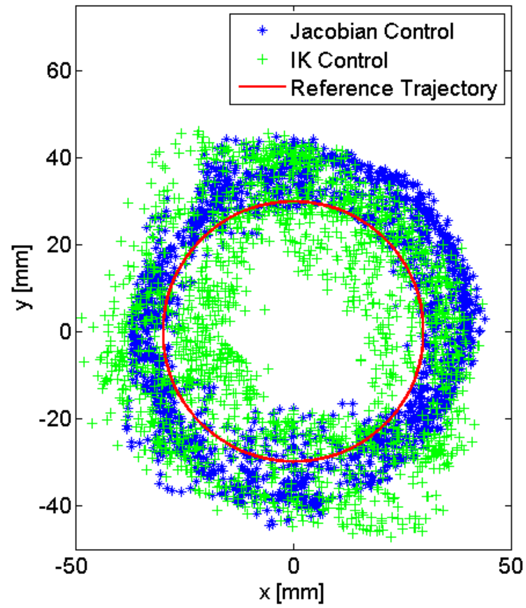

Fig. 11. The actual and reference joint trajectories of the 4-DoF manipulator end effector carrying 80 g of payload when using the IK versus Jacobian control.

troller was a direct inverse kinematics (IK) based controller. Because we were using a 4-DoF manipulator in 6-DoF space, we ignored the z-position and z-rotation of the end-effector. For simplicity, we assumed that the rotational components of the final position are 0 (the platform is level). From there, we used the kinematic model to determine all the joint angles and resulting positions that satisfied those conditions. We used this data to fit a series of polynomial functions relating a desired end-effector position to required angles for each joint. Our IK controller used these functions to calculate all 4 required angles, and use the controller in (5) to reach the target.

The second controller used a geometric Jacobian approach similar to the one presented in Section III-A. Using the kinematic model, we developed linearized Jacobian matrix equations relating changes in joint angles to changes in actuator length (6) and end-effector position (7), respectively:

$$d\vec{L} = \mathbf{A}d\vec{\theta}, \tag{6}$$

$$d\vec{x} = \mathbf{B}d\vec{\theta}, \tag{7}$$

where $\vec{L}$ is the vector of actuator lengths, $\vec{\theta}$ is the vector of joint angles, $\vec{x}$ is the end effector position, and $\mathbf{A}$ and $\mathbf{B}$ are the linearized Jacobian matrices. Just like (4), $\mathbf{A}$ and $\mathbf{B}$ were linearized at $\vec{\theta} = \begin{bmatrix}0 & 0 & 0 & 0\end{bmatrix}^T$. We multiplied (7) by the pseudo-inverse of $\mathbf{B}$ on the left, and substituted into (6) as:

$$d\vec{L} = \mathbf{A}\mathbf{B}^{+}d\vec{x}, \tag{8}$$

which was combined with (1), yielding:

$$\vec{u}(t) = \vec{u}(t - \Delta t) + \mathbf{A}\mathbf{B}^{+}K(\dot{e}_{\vec{x}} + De_{\vec{x}}), \tag{9}$$

where $\vec{u}$ is the control input to each actuator, $\dot{e}_{\vec{x}}$ is the change in error for each controlled value of the end-effector position, $e_{\vec{x}}$ is the end-effector position error, and K and D are scalar control coefficients. This controller requires calculating the forward kinematics of the manipulator within the control loop, but this was observed to not reduce performance.

TABLE II

MEAN AND STANDARD DEVIATION OF THE RADIUS OF THE CIRCULAR END-EFFECTOR TRAJECTORY.

	No Payload	80 g Payload
IK	32 ± 5.8 mm	32 ± 8.4 mm
Jacobian	38 ± 5.2 mm	35 ± 4.4 mm

B. Experimental Results

To experimentally compare their performance, we applied the direct IK and Jacobian approaches to the 4-DoF manipulator. For these tests, we had the end effector follow a circle around the origin with a radius of 30 mm at a period of 15 s. The end effector positions for both controllers can be seen in Figure 10 where the IK controller is more accurate than the Jacobian controller, but exhibits a similar level of noise.

There may have been too much information loss when the control matrices were linearized, reducing the fidelity of this controller. On the other hand, doing entirely separate control of the two 2-DoF joints likely introduce additional noise in the IK controller, as both joints separately oscillate around their desired angle combinations. Quantitative analysis of the end-effector trajectories can be seen in Table II, where data is shown in Mean $\pm$ Standard Deviation form.

In addition, we tested both controllers while the manipulator was carrying a payload of 80 g, the end-effector data for which can be seen in Figure 11. With 80 g of payload, IK controller still follows the desired trajectory with similar accuracy, but the noise in the data increases. It is likely that the additional mass amplifies the dynamic effects of the 6 valves operating simultaneously. On the other hand, the noise of the Jacobian controller did not change significantly, though the motion of the end-effector remained outside of the desired trajectory.

V. Conclusion and Future Work

We developed a new soft pneumatic actuator that was both more reliable and easier to fabricate and use. Three of these new actuators were employed to drive a 2-DoF universal joint module, reducing the required pneumatic and electronic infrastructure. We derived a Jacobian-based iterative sliding mode controller to control the module, and demonstrated its effectiveness in following step functions and sinusoidal trajectories. We mounted two of these modules in series to create a 4-DoF soft-actuated manipulator.

We stuedied two motion control approaches for this 4-DoF manipulator: a direct IK enabled controller, which calculated desired joint angles and ran the 2-DoF controller separately for each joint, and an end-effector Jacobian controller, which directly related the end effector position error to a required change in control input. We tested these controllers when following a circular end-effector trajectory and found that the Jacobian controller was more precise (especially under additional payload), while the IK controller was more accurate.

We observed both qualitatively and in the data (Figure 5) that the lower joint had more difficulty following trajectories. This is likely because of the additional weight resting upon it, but it brings up some interesting questions regarding soft actuated manipulator design. We conclude that, for improved performance, a soft actuated manipulator should have different actuators and geometries (including the amount of pre-strain) at each joint to fulfill their individual force and workspace requirements. This could result in a manipulator design optimization similar to our recent work in [12].

One of the problems that this modular manipulation system faced was with oscillations in the joints, and correspondingly, the end-effector position. This is primarily the result of the PWM duty cycles of each of the valves creating dynamic effects that ripple though the system. It was observed that higher-magnitude oscillations would often occur at the exact same part of a repeating trajectory over multiple cycles. We are currently unable to predict this behavior, but one way to lessen their effects would be to increase the PWM signal frequency. In addition, we are looking into the possibility of using separate valves to control the inlet and outlet of each actuator, which would allow us to more completely control the system and allow for full-stop capability at the cost of doubling the driver signals required.

Despite the reduction in pneumatic infrastructure (compared to an antagonistic control configuration) involved in controlling 2 degrees of freedom with 3 rPAMs, it is still a redundant system. The geometric Jacobian control method only calculates changes in control inputs to each actuator until the desired angles are reached, meaning that the initial control inputs (or a common pressure offset for all rPAMs) represent a missing degree of control. Differing initial control inputs will result in different pressure combinations at the goal state. This was used to increase the performance of the lower joint in the 4-DoF manipulator; we increased the initial input to reduce a behavior where the joint would pass over an axis and overshoot before being caught by the other actuator. We would like to investigate this behavior in greater detail.

Acknowledgment

The authors would like to thank Yixiao Pan and Joe St. Germain for their help with the fabrication and assembly of the soft-actuated module.

References

[1] Y.-L. Park, S. J, G. K, E. C, Goldfield, and W. R.J, "A soft wearable robotic device for active knee motions using flat pneumatic artificial muscles," in *Robotics and Automation (ICRA), 2014 IEEE International Conference on*, pp. 4805–4810, IEEE, 2014.

[2] F. Renda, M. Cianchetti, M. Giorelli, A. Arienti, and C. Laschi, "A 3d steady-state model of a tendon-driven continuum soft manipulator inspired by the octopus arm," *Bioinspiration & biomimetics*, vol. 7, no. 2, p. 025006, 2012.

[3] T. Nakamura, Y. Akamatsu, and Y. Kusaka, "Development of soft manipulator with variable rheological joints and pneumatic sensor for collision with environment," *Journal of Robotics and Mechatronics*, vol. 20, no. 4, p. 634, 2008.

[4] K. Boku and T. Nakamura, "Development of 3-dof soft manipulator with er fluid clutches," *Journal of Intelligent Material Systems and Structures*, vol. 21, no. 15, pp. 1563–1567, 2010.

[5] A. D. Marchese, K. Komorowski, C. D. Onal, and D. Rus, "Design and control of a soft and continuously deformable 2d robotic manipulation system," in *Proceedings of IEEE International Conference on Robotics and Automation*, 2014.

[6] B. Tondu, S. Ippolito, J. Guiochet, and A. Daidie, "A seven-degrees-of-freedom robot-arm driven by pneumatic artificial muscles for humanoid robots," *The International Journal of Robotics Research*, vol. 24, no. 4, pp. 257–274, 2005.

[7] G. Tonietti and A. Bicchi, "Adaptive simultaneous position and stiffness control for a soft robot arm," in *Intelligent Robots and Systems, 2002. IEEE/RSJ International Conference on*, vol. 2, pp. 1992–1997, IEEE, 2002.

[8] S. Eskiizmirliler, N. Forestier, B. Tondu, and C. Darlot, "A model of the cerebellar pathways applied to the control of a single-joint robot arm actuated by mckibben artificial muscles," *Biological cybernetics*, vol. 86, no. 5, pp. 379–394, 2002.

[9] P. van der Smagt, F. Groen, and K. Schulten, "Analysis and control of a rubbertuator arm," *Biological Cybernetics*, vol. 75, no. 5, pp. 433–440, 1996.

[10] J. Schröder, K. Kawamura, T. Gockel, and R. Dillmann, "Improved control of a humanoid arm driven by pneumatic actuators," *Proceedings of Humanoids 2003*, 2003.

[11] E. H. Skorina, M. Luo, S. Ozel, F. Chen, W. Tao, and C. D. Onal, "Feedforward augmented sliding mode motion control of antagonistic soft pneumatic actuators," in *Robotics and Automation (ICRA), 2015 IEEE International Conference on*, pp. 2544–2549, IEEE, 2015.

[12] M. Luo, E. H. Skorina, W. Tao, F. Chen, and C. D. Onal, "Optimized design of a rigid kinematic module for antagonistic soft actuation," in *International Conference on Technologies for Practical Robot Applications (TePRA)*, IEEE, 2015.

[13] M. Luo, Y. Pan, E. Skorina, W. Tao, F. Chen, S. Ozel, and C. Onal, "Slithering towards autonomy: a self-contained soft robotic snake platform with integrated curvature sensing.," *Bioinspiration & biomimetics*, vol. 10, no. 5, pp. 055001–055001, 2015.

[14] M. Luo, Y. Pan, W. Tao, F. Chen, E. H. Skorina, and C. D. Onal, "Refined theoretical modeling of a new-generation pressure-operated soft snake," in *International Design and Engineering Technical Conferences & Computersand Information in Engineering Conference (IDETC/CIE 2015)*, ASME.

[15] M. Luo, M. Agheli, and C. D. Onal, "Theoretical modeling and experimental analysis of a pressure-operated soft robotic snake," *Soft Robotics*, vol. 1, no. 2, pp. 136–146, 2014.